ISTITUTO NAZIONALE DI FISICA NUCLEARE

Laboratori Nazionali di Frascati

INFN-21-02/LNF
26 Maggio 2021

Crilin: CRystal calorImeter with Longitudinal InformatioN for a future Muon Collider

Eleonora Diociaiuti[1], Daniele Paesani[2], Alessandro Saputi[1], Ivano Sarra[1], Diego Tagnani[3]
[1)] *INFN, Laboratori Nazionali di Frascati, Via Enrico Fermi 54, 00054 Frascati, Italy*
[2)] *INFN, Sezione di Bari e Università degli Studi di Bari, Via Orabona 4, 70126 Bari, Italy*
[3)] *INFN, Sezione di Roma Tre, Via della Vasca Navale 84, 00146 Roma, Italy*

Abstract

Being modern tracking systems very precise, jet performance in particle flow-like reconstruction algorithms is usually limited by the calorimeter performance. In particular, a high granularity is required in order to distinguish signal particles from background and to solve the substructures necessary for jet identification. Time of arrival measurements in the calorimeter could play an important role in HL-LHC, since a high number of pile-up collisions is expected, and the timing could be used to assign clusters to the corresponding interaction vertex. In a Muon Collider, the timing could be used to remove signals produced by beam-induced background, asynchronous with respect to the bunch crossing. The calorimeter energy resolution is also fundamental to measure the kinematic properties of jets: a finely segmented calorimeter design should be favored in order to solve the jet substructure. However, this contrasts with the requirement for high timing resolution even for signal events involving low energy deposits, such as in the case of high impulse muons. Our proposed design, the Crilin calorimeter, is a semi-homogeneous calorimeter based on Lead Fluoride (PbF_2) Crystals readout by surface-mount UV-extended Silicon Photomultipliers (SiPMs). In this paper, the development of a small prototype consisting of 2 layers of 3×3 crystals each is reported along with the relative results.

Published by
Laboratori Nazionali di Frascati

1 Introduction

Calorimeters are generally divided in two categories, homogeneous and sampling. The best compromise between the two technologies is sought in order to optimize experimental requirements and minimize the drawbacks associated with the limitations of standard solutions . The most recent technological developments allow this rigid distinction to be abandoned in favour of novel architectures: the Crilin calorimeter is a semi-homogeneous calorimeter based on Lead Fluoride (PbF_2) crystals readout by surface mounted UV extended Silicon Photomultipliers (SiPMs). The Crilin calorimeter can be segmented longitudinally as a function of the energy of the particles and of the background level, thanks to its modular design which enables a high degree of reconfigurability. The Crilin R&D proposal embeds a modular architecture based on stackable submodules composed of matrices of crystals, in which each crystal is individually readout by 2 series of 2 UV-extended surface mount SiPMs. Crystal dimensions are $10 \times 10 \times 40$ mm^3 and the surface area of each SiPM is 4×4 mm^2, so as to closely match the crystal surface. In Figure 1, a Geant4 geometry involving 10×10 modules of PbF_2 crystals is shown.

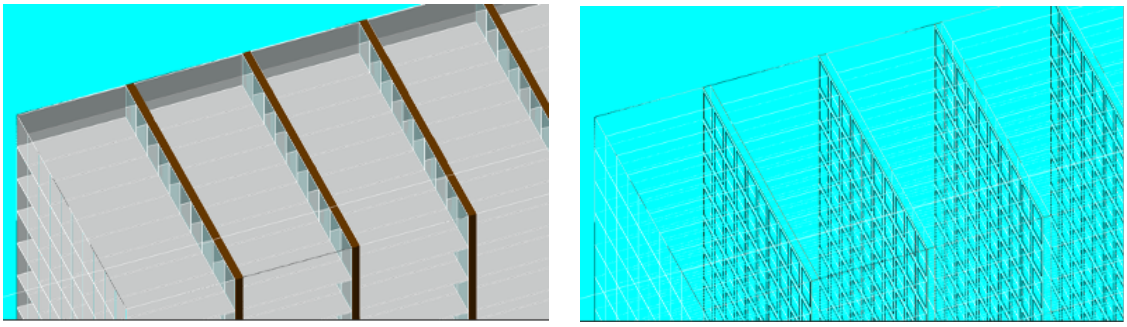

Figure 1: Geant4 geometry of the 10x10 calorimeter with 5 modules: PbF_2 crystals (grey) and SiPMs layers (brown) are shown.

The intrinsic advantage of this architecture consists in the excellent compromise of the following requirements:

1. high response speed (the Cherenkov response of PbF_2 is instantaneous with respect to the particle passage);
2. reduced signal width and therefore an excellent ability to resolve temporally close events at high rate (good pileup capability);
3. good light collection enabling good energy resolution throughout the whole dynamic range;
4. good resistance to radiation;
5. fine granularity and scalable SiPMs pixel dimensions.

The test and results shown in the following have been obtained with PbF2 crystals from SICCAS [1] and S14160-4050HS SiPMs from Hamamatsu [2].
Pixel size and SiPM gain are tailored according to the energy range required by the expected experimental conditions. The extremely high granularity allows a maximum energy deposit per crystal in the order of 3-5 GeV, which corresponds to the simulated deposit associated with 30 GeV π^0 events. In Figure 2 (left), the energy deposited in each one of the modules - averaged over 10^3 simulated 30 GeV π^0 events - is reported . In the simulated detector geometry, 5 modules housing 40 mm long crystals are implemented.In this regard, the choice of 50 um pixels would guarantee an excellent linearity in the response.
Moreover, the Light Yield (LY) of the system should be high enough to enable a good measurement of the energy deposited by the passage of high p_T muons, which - according to our simulations - should correspond to an average deposit of 30-40 MeV per crystal, as shown in Figure 2 (right).

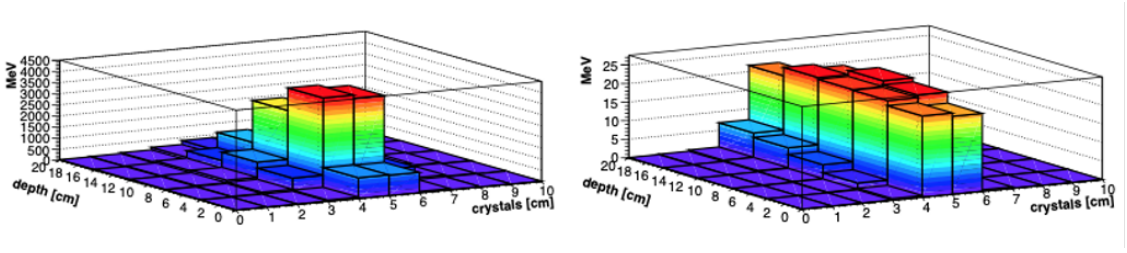

Figure 2: Energy deposited per module in a 10x10 calorimeter with 5 modules: average deposition of one thousand 30 GeV π_0 (left) and negative muons (right).

As far as timing resolution is concerned, in this configuration the stochastic term linked to PbF_2 would be practically negligible, while the dominant contribution would instead be linked to the rise time of the signal. The rise-time of SiPM pulses is in the order of nanoseconds, while the rise-time of the FEE depends on the choice of the amplifier and shaper. Assuming a total rise-time of approximately 3-5 ns for the SiPM and FEE, the achievable time resolution would be of the order of 3-5 ns/$\sqrt{Np.e.}$. This corresponds to 300 ps in the case of high impulse muons and up to 50 ps in the case of pions and jets, as discussed in Sec. 2.

1.1 Radiation environment and radiation damage

Modern HEP experiments are associated with harsh radiation environments, due to the rising need for higher intensities. This sets the minimum performance requirements to be guaranteed by the Crilin calorimeter. For example, in the case of a future Muon Collider [3], the requirements relative to the barrel electromagnetic calorimeter (EMC) involve a 1 Mrad total ionising dose (TID) and a 10^{12} n_{1MeV}/cm^2 equivalent neutron fluence. Moreover, with regards to the EMC for the future upgrade of the Mu2e experiment, Mu2e-II [4], the fluence requirement for the photosensors is even more demanding, and

involves a 10^{13} n_{1MeV}/cm^2 target fluence. Our goal is to satisfy all stated requirements with the design and development of Crilin.
With regards to Total Ionising Dose (TID) effects, the radiation hardness of PbF2 was evaluated in different test campaigns with integrated doses up to the Mrad range [5], [6]. A reduction of the light yield around 10-20$\%$ is generally observed and associated with a decreased transmittance, ensuing the appearance of radiation-induced absorption bands due to the formation of colour centres [7], [8]. As far as neutron damage is concerned, the resistance of crystals against displacement damage dose (DDD) is well documented in literature [5]. Our results relative to transmittance deterioration after irradiation with either photons from ^{60}Co or with 14 MeV neutrons are reported in Sec. 3.
Further regarding neutrons, SiPMs are the component which are most subject to their detrimental effects, mainly in terms of a fluence-dependent dark current increase. At room temperatures indeed, the exposure of a 1 cm^2 SiPM to a 10^{12} n_{1MeV}/cm^2 fluence leads to an increase in the dark current from the μA level up to tens of mA [9], which represents a dominant contribution to the noise level of the instrument. Moreover,the increased dissipated power ($P = I_{dark} \times V_{bias}$) and the ensuing heating effect will result in a modification of the SiPM operating point, with an associated alteration of its gain. An effective countermeasure to reduce the dark current and stabilise the operating point of the photodetector is represented by thermalising the whole SiPMs layer to very low temperatures. A 10 °C temperature drop corresponds indeed to a reduction of the dark current by a factor of 3. Cooling SiPMs down to 0 °C allows instead a current reduction by a factor of about $3^{2.5} \sim 15$ [9].
As a result, in the Crilin prototype, a cooling system based on the fluxing of dry cold gas was implemented. To prevent condensation on the SiPMs surface by lowering the dew point, the whole crystal and SiPM compartment is saturated with a nitrogen atmosphere. Each module - which houses a single layer composed of 9 crystals, along with the respective SiPMs and FEE board - can be disassembled and serviced individually, as reported in Sec. 4.

2 Light Yield Measurement

In order to carry out a preliminary evaluation of the light yield, the energy response of PbF_2 to cosmic rays was measured using a single crystal ($10 \times 10 \times 40$ mm^3), optically coupled - by means of UV clear optical grease - with two 4×4 mm^2 SiPMs connected in a series configuration. The crystal was wrapped with a single layer of 100 μm thick Mylar foil. For this test, the polarization of the SiPMs series was performed using a TTi PLH250-P power supply, and a custom transimpedance amplifier, providing an equivalent 250 charge gain, was used to amplify the light pulses. Thanks to the high gain of the amplifier, the charge associated with a single photoelectron could be measured, as shown in Figure 3. This value was used to scale the Minimum Ionizing Particles (MIP) charge response, shown in Figure 4, and thus to determine the relative number of photo-electrons.

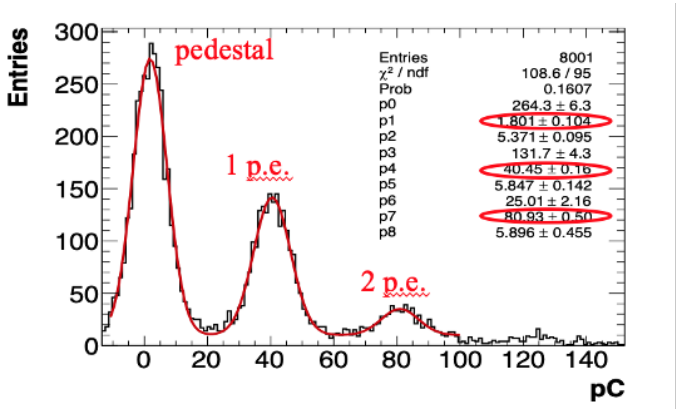

Figure 3: Charge in pC corresponding to 1 and 2 photo-electrons in randomly gated acquisitions of the SiPMs series dark counts.

MIP acquisitions were performed in self triggering mode and the charge distribution was fitted with a Landau distribution. From the most probable value (MPV) of the Landau fit,

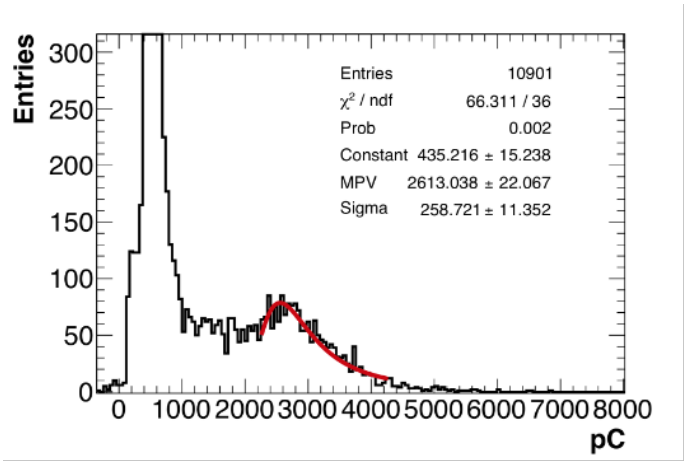

Figure 4: Response to cosmic rays in self triggering mode: measured charge response for MIPs.

the number of photoelectrons is calculated as:

$$N_{p.e.} = \frac{2600pC}{40pC \cdot dE/dx} = 65p.e./(dE/dx) \tag{1}$$

where 40 pC is the charge corresponding to one single photo-electron. From our Monte Carlo simulations, the MPV corresponding to an energy loss of dE/dx = 11 MeV was evaluated, from which, in turn, a light yield of 6 p.e. / MeV is derived.
This number can be compared with the results obtained with the SAC calorimeter [6], which relies on the same type of crystals. In the case of SAC indeed, a LY equal to 2 pe/MeV was measured by integrating the signal collected for wavelengths greater than 300 nm with a R13478Q PMT, having 15-20% QE between 300-450 nm, and with a collection in the area of 40% (value which is comparable with the 32% coverage of our

test). Since our UV-extended SiPMs allow the collection of a broadened spectral range of Cherenkov Light - with a 30-40% PDE from 300 to 450 nm - an improvement by a factor of two in the LY can be expected for our prototype. Thanks to simulations, we can indeed estimate that this extended spectral sensitivity corresponds to a doubling in the global LY of the system, which furthermore relies on crystals wrapped with Mylar foil, instead of the black Tedlar used in the SAC calorimeter. Thus, our measurement of 6 p.e./MeV looks in good agreement with these extrapolations.

3 Crystals Characterization

The characterization campaign of PbF_2 crystals was started in February 2021 at the National Laboratories of Frascati. The crystals, produced by SICCAS, have a 40 mm length, with 5×5 mm^2 square faces. After the evaluation of the light yield (as described in Sec. 2), two crystals were used to evaluate the radiation hardness of PbF_2 , by comparing their transmittance before and after irradiation. The latter was carried out with either photons or neutrons. The totality of the crystals used for the irradiation tests were randomly selected from the main production batch of the Crilin prototype, so as to guarantee consistent results with the final instrument.
The first crystal was tested without any kind of wrapping (in the following it will be referred to as the "naked" one), while the second one (shown in Figure 5) was wrapped with a 100 μm thick Mylar foil.

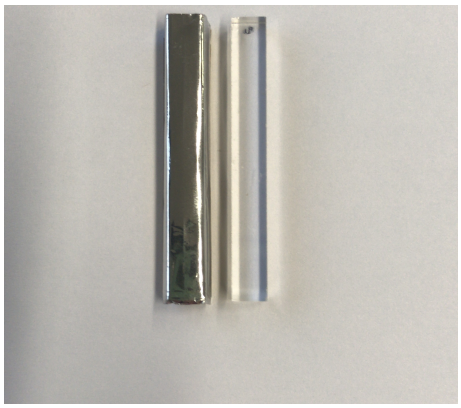

Figure 5: The two PbF2 crystals used during the characterization. Left: Al Mylar wrapping. Right: "Naked"crystal.

Transmittance measurements were performed before and after each irradiation run. Crystals were irradiated both at Calliope Facility of ENEA Casaccia [10] using photons from ^{60}Co and at the Frascati Neutron Generator (FNG) facility of ENEA Frascati [11] using 14 MeV neutrons. Longitudinal transmission spectra were acquired for each crystal as a function of the wavelength λ in the 210 - 700 nm range, with 1 nm steps. The transmittance of the three crystal specimens was measured using a PerkinElmer Lambda 950 UV/VIS dual beam spectrometer [12]. In this case, the optical transmittance can be ob-

tained as follows:

$$T = \frac{\frac{S-D}{Ref-D}}{\frac{S_0-D_0}{Ref_0-D_0}} \tag{2}$$

S, D and Ref are respectively the measured, reference and dark signals while the subscript 0 refers to the baseline measurement performed without the crystal inside the spectrometer. Figure 6 shows the experimental setup: yellow lines represent the incident and the outgoing beam. Before starting the transmittance measurement, a reproducible test is

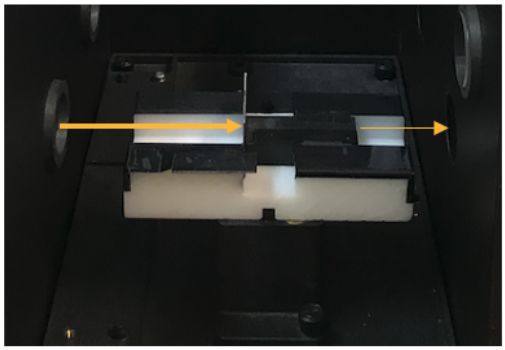

Figure 6: PbF_2 crystal before the measurement of the longitudinal transmittance.

performed removing and relocating the crystal on the sample holder for each acquisition. The obtained spectra are reported in Figure 7 (Left). The spread at each wavelength can be evaluated as:

$$\sigma = \frac{T_{max} - T_{min}}{T_{max}} \tag{3}$$

Where T_{max} and T_{min} are respectively the maximum and minimum transmittance value of the set of measurements. As shown in Figure 7 (Right) a value of $\sigma = 1.1\%$ is associated with the longitudinal transmittance measurement. After the reference transmittance

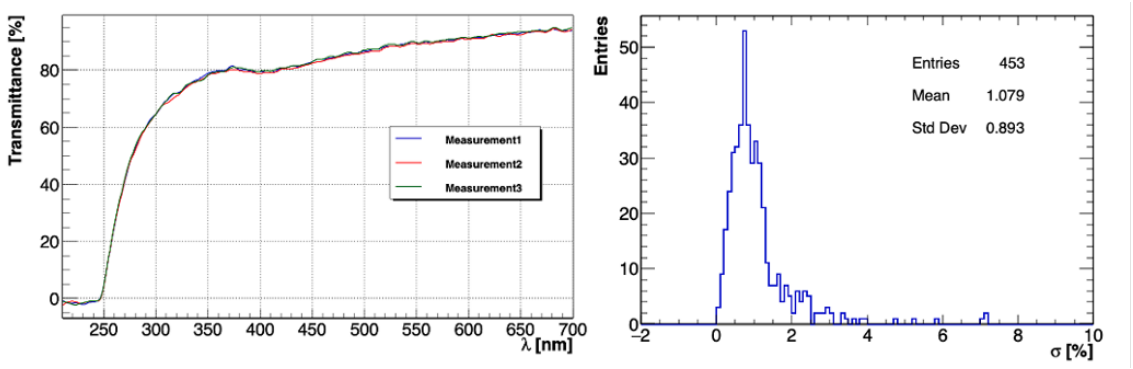

Figure 7: Longitudinal transmittance measurement on "naked" crystal (Left). σ values for repeated longitudinal transmittance measurements performed removing and replacing the crystal on the holder (Right).

measurements, the irradiation phase was started in Calliope, a pool-type gamma irradiation facility equipped with a ^{60}Co radio-isotopic source array housed in a large volume

($7.0 \times 6.0 \times 3.9$ m^3) shielded cell. The source rack is composed of 25 ^{60}Co source rods (with an active area of 41×90 cm^2) arranged in a planar geometry (see Figure 8), producing photons with $E_\gamma = 1.25$ MeV.

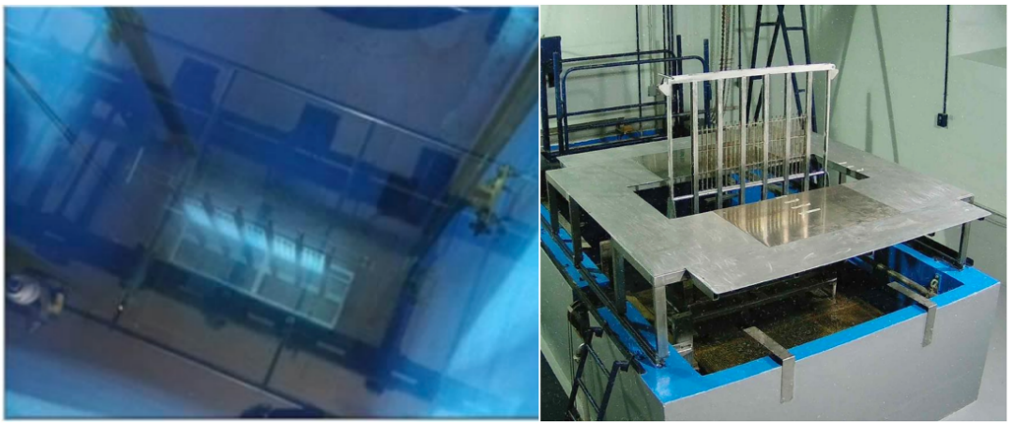

Figure 8: Calliope rack with ^{60}Co sources (Left). Irradiation cell with ^{60}Co sources rack and the platform for sample positioning (Right).

The activity for the Calliope plant was 1.97×10^{15} Bq at the time in which the measurements were conducted. The two crystals were positioned at a 70 cm distance from the source, corresponding to 100 krad/h dose rate. The transmittance measurements were performed at different steps of the irradiation, which took place in three days for a total absorbed dose of 4.4 Mrad. The longitudinal transmittance obtained at each step of irradiation is reported in Figure 9. After a 30 krad dose exposure, a significant deterioration in transmittance can be seen for wavelengths below 300 nm, along with an almost constant 25% drop for wavelengths above 300 nm. A transmission recovery of 10% is observed at 350 nm after one day of natural annealing in the dark. Any further deterioration of the transmittance after a TID approximately equal to 20 Mrad is completely negligible, indicating a saturation effect associated with the damage mechanism. This is especially true for crystals wrapped with Mylar (Figure 9).

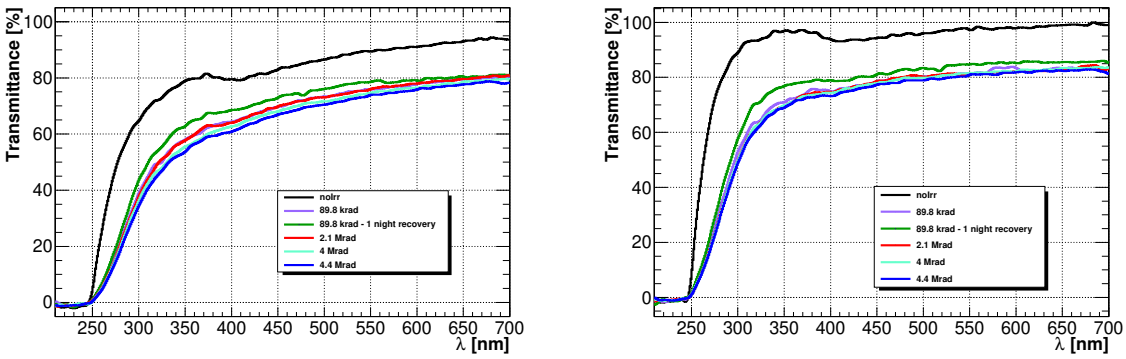

Figure 9: Longitudinal transmission at different steps of irradiation for "naked" crystal (left) and Mylar wrapped crystal (right).

After the irradiation phase, the crystals were kept in a dark box to allow natural recovery, as described in [5]. In Figure 10, the spectra at different steps of the recovery process are reported. A transmission recovery of 15% is observed above 300 nm after 18 days of natural annealing since irradiation. To further improve the recovery process, a light-bleaching test on the irradiation crystals with 400 nm blue light was performed in May 2021 by the Crilin group, according to the procedures and methods described in [13].

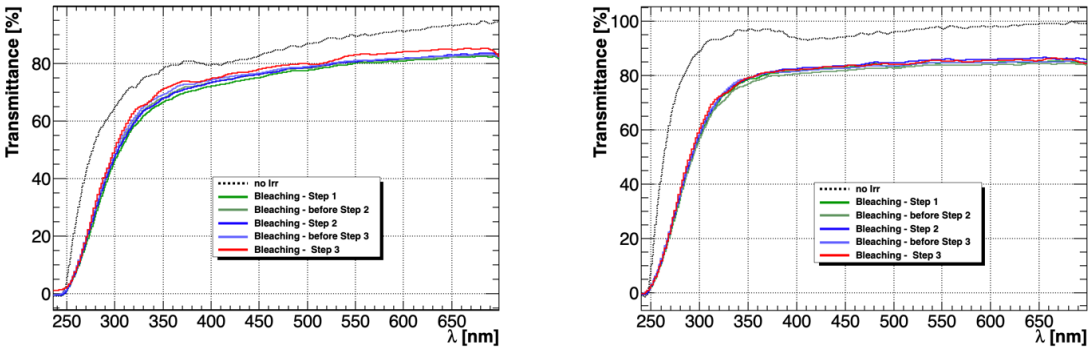

Figure 10: Transmission spectra obtained at different recovery steps for the "naked" crystal (left), the crystal with Mylar wrapping (right).

After 16 hours of optical bleaching, a modest recovery of a few percent on the transmittance spectrum was observed, indicating a small accelerating effect on the recovery process with respect to the previously described natural annealing case. After the optical bleaching step, crystals were irradiated with neutrons at FNG. Neutron generation at FNG is based on the T(d,n)α fusion reaction, producing 14 MeV neutrons with a flux up to 10^{12} neutrons/s in steady state or pulsed mode. In Figure 11, the neutron spectrum is shown as a function of the fluence.

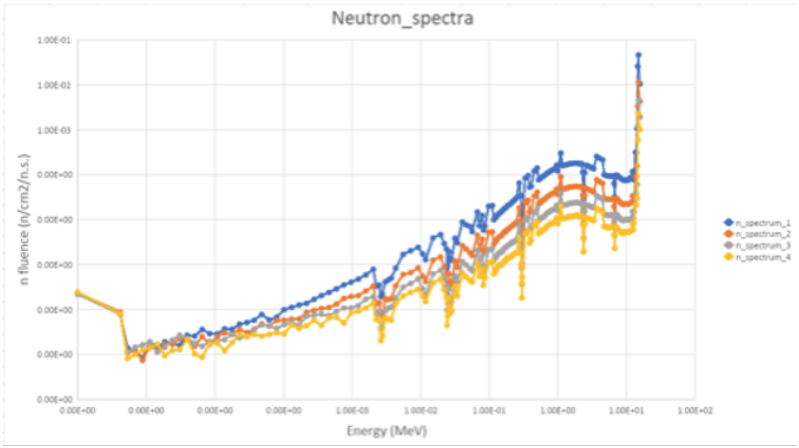

Figure 11: FNG neutron spectra as a function of the fluence.

The crystals under test, as shown in Figure Y, were placed at 1 cm from the source (relatively to their front face). The respective SiPMs were instead placed against the crystal's

back faces. Figure 12 reports the neutron flux map in the FNG facility. In order to better evaluate the expected neutron fluences, a simulation of the irradiation process was implemented on the McStas simulation package [17], using 1 cm bins along the crystal's axes.

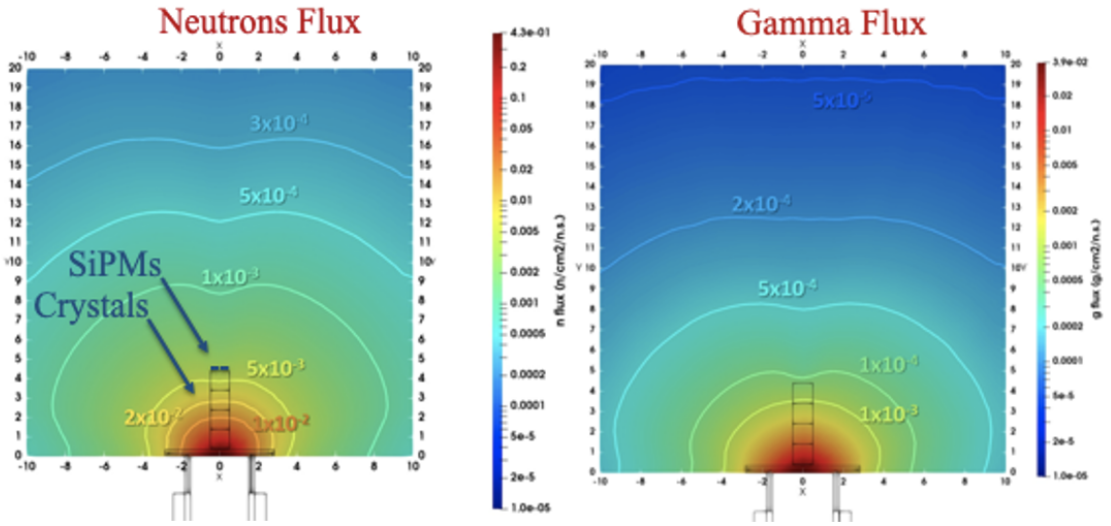

Figure 12: Simulation of the neutrons (left) and gamma (right) flux: crystals were placed at 1 cm from the source with the SiPM positioned on the back face.

In about 1 hour and 30 minutes of irradiation with 14 MeV neutrons, a total 10^{13} n/cm^2 fluence was delivered to the first 1 cm segment of the crystals, while SiPMs received a fluence of 5×10^{11} n/cm^2. As shown in Figure 12 (right), the gamma flux associated with the irradiation process resulted in a (negligible) 1 Gray TID for crystals. The 10^{13} fluence corresponds to a 1.8×10^{13} n_{1MeV} equivalent fluence. After irradiation, crystals were shipped to Enea Casaccia to perform a new series of transmittance measurements. The results are shown in Figure 13: a significant reduction of the transmittance below 400 nm is observed; an almost constant 10% reduction is observed above 400 nm. From the convolution of TID and NIEL damage we could conclude that a factor 2-3 of the light is expected in the first Layer of Crilin calorimeter. Thanks to dedicated transversal transmittance studies we will evaluate if the damage is considerably uniform along crystal axes or , as expected, mainly localized in the first centimeters of the front face, and how this will impact the LRU of the system.

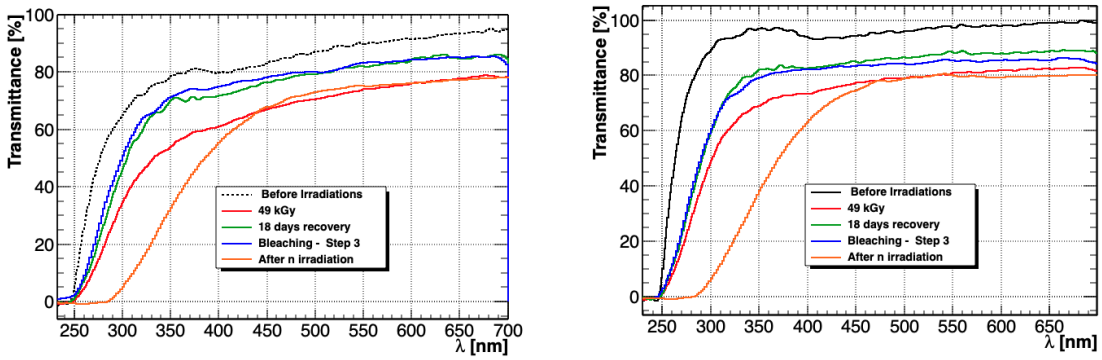

Figure 13: Transmission spectra obtained after the irradiation of 10^{13} n/cm^2: "naked" crystal (left), the crystal with Mylar wrapping (right).

3.1 Radiation damage on SiPM

As explained in Section 1.1, the main effect on SiPMs associated with neutron fluence is represented by an increase in the dark current. The leakage current as a function of V_{bias} at 25 °C for the series of two irradiated SiPMs is reported in Figure 14. The ratio of the dark currents, after and before the irradiation with 9×10^{11} n_{1MeV}/cm^2 on SiPMs is 11 mA / 2 μA = 6000, evaluated at the nominal bias point (41.35 V per SiPM, 82.7 V per series). The expected leakage current for a 0 °C operating point is less than 1 mA per series, compatible with our mechanical and electrical specifications, as discussed in Sections 4 and 5.

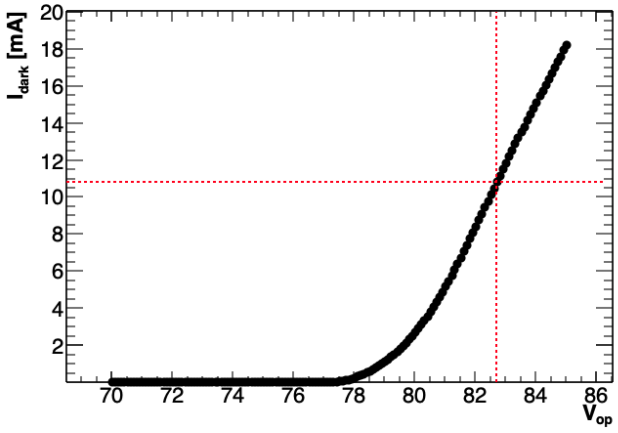

Figure 14: Dark current versus applied bias voltage for the series of the two irradiated SiPMs.

4 Mechanical Design

This section describes the mechanical components of the Crilin prototype, along with the integration of electronic boards and the cooling system.

In the current design, the prototype consists of two submodules, each composed of a 3-by-3 crystals matrix. The submodules are arranged in a series and assembled together by screws, resulting in a compact and small calorimeter (Figure 15).

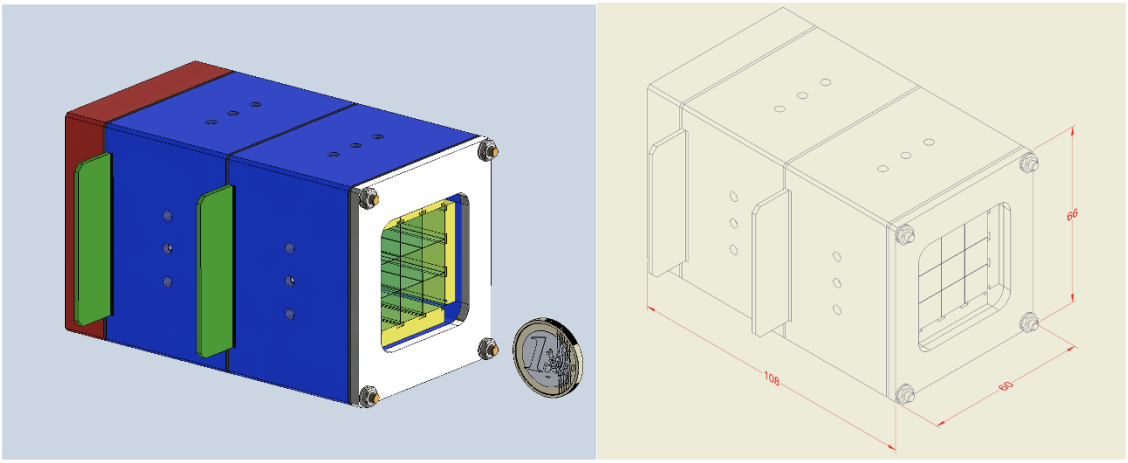

Figure 15: CAD model of Crilin Prototype (left) and total dimensions (right).

Each crystal matrix is housed in a light-tight case which also embeds the front-end electronic boards and the cooling system. The mechanical architecture of Crilin comprises the following key elements:

- The cases (Figure 16), which house the crystal matrix and embed the front-end electronic boards. They are manufactured in aluminium alloy (EN AW 6082) and ABS to ensure thermal insulation.

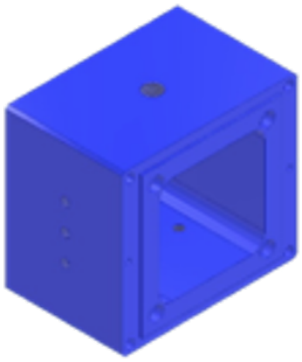

Figure 16: CAD model of the crystals case.

- The locking plates, to which the positioning and blocking of crystals is entrusted, are manufactured in ABS. This solution eases the assembling, positioning and locking of the crystals matrix. The assembled prototype - comprising 2 modules of 9 crystals each, is shown in Figure 17, along with the relative locking plates.

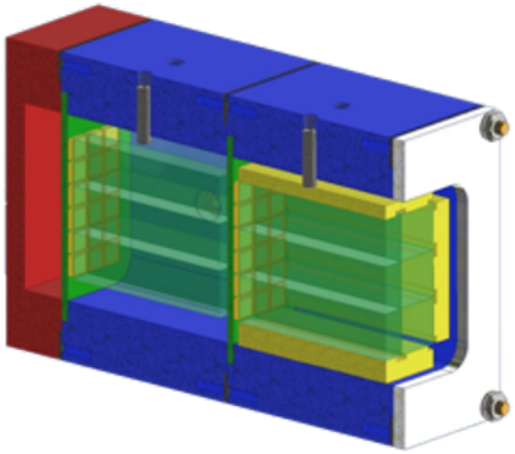

Figure 17: CAD model of the locking plates.

- The hydraulic connectors, transporting the cooling gas into the individually sealed modules as shown in Figure 18.

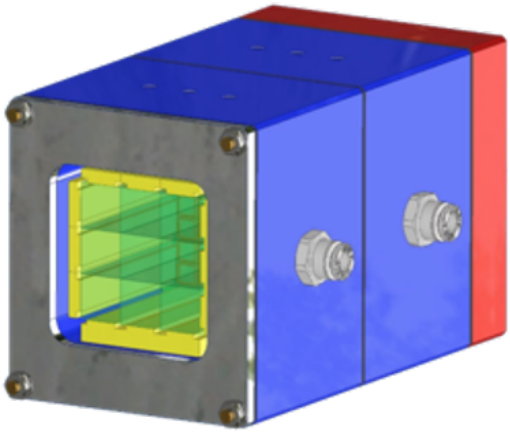

Figure 18: CAD model of the assembled calorimeter, including the hydraulic connectors needed to flux cold gas inside the active volume of the prototype and to prevent condensation.

- The seals, which make each submodule light-tight, are shown in Figure 19.

4.1 Cooling System

The on-detector electronics and SiPMs must be cooled during operation, so as to improve and stabilise the performance of SiPMs against irradiation, as stated in Section 2. Our design is capable of removing the heat load due to the increased photosensor currents after exposure to the expected 10^{12} n_{1MeV}/cm^2 fluence, along with the power dissipated by the

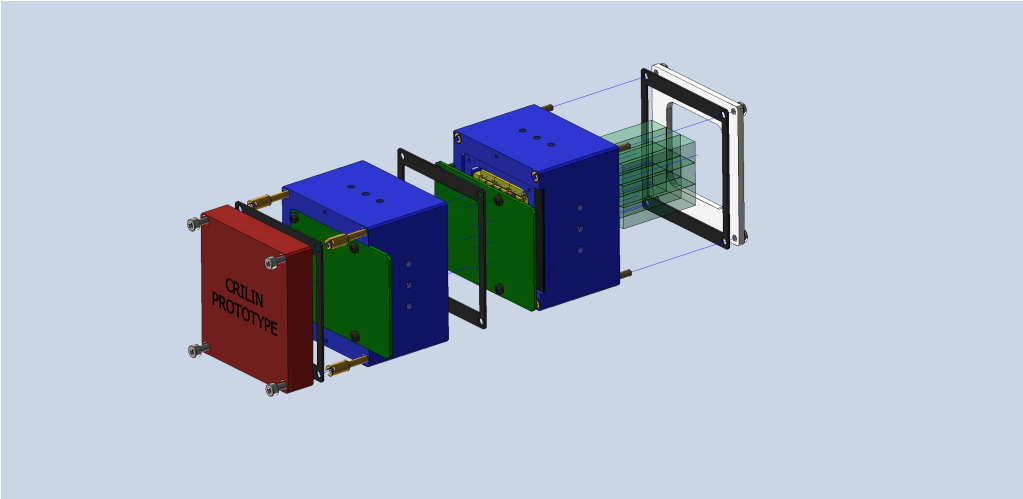

Figure 19: 3D model of the cross section of the prototype parts.

amplification circuitry. The total heat load was estimated as 350 mW per channel. The Crilin cooling system, which is based on conduction and forced convection of nitrogen, will provide the optimum operating temperature for the electronics and SiPMs at around 0 °C . In Figure 17 the schematic of the cooling system is shown. Gas fluxing will also prevent any condensation on SiPM or crystal surfaces.

5 Electronics

Each calorimeter submodule is composed of a 3-by-3 matrix of PbF_2 crystals. Each crystal is in turn individually readout by a square matrix of 4 SiPMs in surface-mount technology, connected in two series of 2 photosensor each. Each series of 2 SiPMs (Hamamatsu S14160-4050HS) is independently processed by a separate low-noise amplification stage. This architecture was implemented in order to increase the reliability of the system through redundancy and improve its time resolution thanks to the use of two detectors per crystal.
All SiPMs contained in each submodule are biased using a common positive supply generated externally and distributed to all channels after filtering, provided by C3, C4 and R6 (Figure 20). As a result, gain equalisation is performed offline after signal acquisition. This architecture was implemented due the small spread in the breakdown voltages of the SiPMs contained in each matrix, which are carefully matched. The overall RMS spread in breakdown voltages for all 72 SiPMs installed in the prototype is 6.3 mV. The nominal breakdown voltage for the photosensors is 38,6 V. The operating point for SiPMs was chosen with a nominal 2.7 V overvoltage, corresponding to a gain of 2.5×10^6.
The PCB layout was conceived so that, for each crystal, the amplification and bias distribution circuitry - mounted on the bottom side - could be contained in the footprint of the 4 photodetectors mounted on the top side. The installation of the photodetectors should privilege planarity with respect to the crystal faces, while the amplification

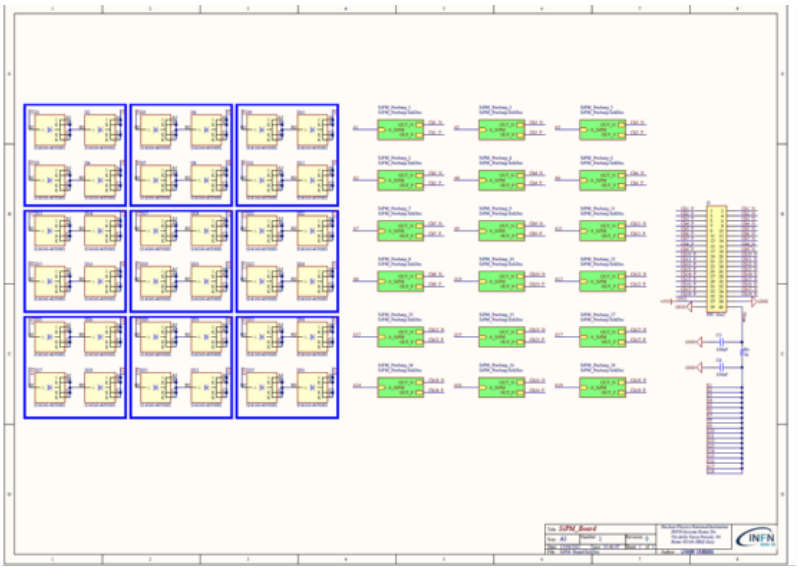

Figure 20: SiPM connection, bias distribution and amplifier blocks for the front-end electronics board.

circuitry should prevent crosstalk, despite the high component density of the PCB. The overall dimensions of the multi-layer PCB are 40x35 mm^2. The chosen PCB solder mask for the final prototype is in black colour, an element which can be beneficial in preventing cross talk from happening at the SiPM-crystal interfaces.

Due to the tight geometrical constraints, integrated high-speed TIAs available in bare chip packages were chosen to be mounted using wire-bonding techniques. The chosen IC is the MAX3664E/D [14] low power transimpedance preamplifier for 622 Mbps SDH/SONET, featuring differential output. It operates from a single 3.3 V supply, with 70 mW power consumption. The chip embeds a DC cancellation circuit to provide a true differential output swing over a wide range of input current levels, thus reducing pulse-width distortion. The differential outputs are back terminated with 50 Ω per side. The nominal transimpedance gain is 8 kΩ . In our case this corresponds to an overall charge gain of about 2.

With reference to the schematic shown in Figure 21, an input resistor (R3) and a compensation network (formed by R2 and C2) were added to suppress input noise and increase stability. The individual 3.3 V supply lines are decoupled and filtered via C1 and R1.

The operating temperature for the opto-electronic section was set at 0 °C . As a result, the heat generated by each SiPM - especially after the increase in dark current due to irradiation - is managed through thermal bridges (Q-Bridge [15]), which are installed on the anode and cathode connections of each SiPM. These connections are replicated on each layer and thick copper pads are used to increase the overall thermal conductivity of the PCB. The board, as shown in Figure 22, is connectorized using a straight FPC 20×2 connector which manages all 18 differential outputs, along with the bias and supply voltages.

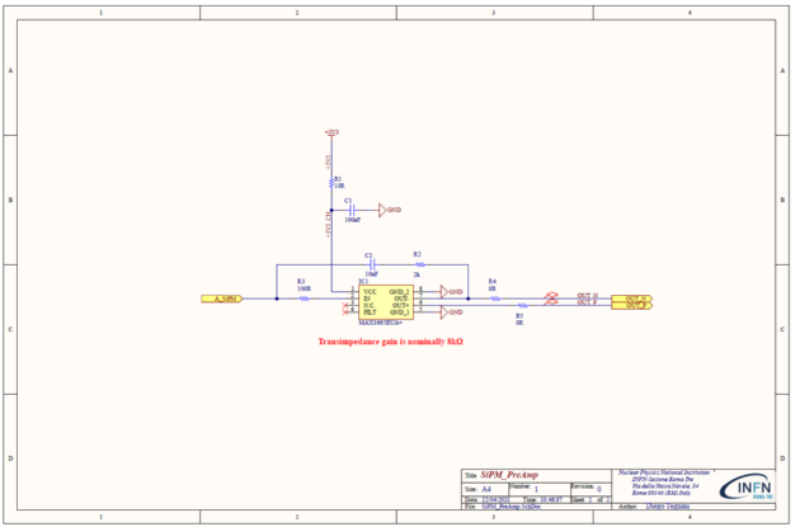

Figure 21: Schematic of the amplification stage with differential output for a single channel.

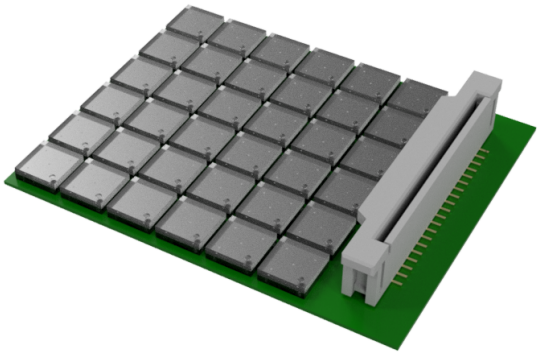

Figure 22: Rendering of the front-end board for a single 9-crystals module of the Crilin prototype.

A control module was developed in standard NIM format to provide the regulated bias supply voltages and perform the conversion of the differential pulses to a single ended, 50 Ω adapted voltage signal. The latter is fed into a fast discriminator with differential current output, to be in turn processed by the TDC. The NIM module also embeds an additional gain 10 stage, which can be enabled to adjust the dynamic range for lower deposited energies during the front-end R&D phase.

6 Module-0 and further development

In order to validate the design choices relative to the opto-electronic,mechanical and cooling architecture of the calorimeter, a small scale prototype with 2 crystals and 4 ampli-

fication channels, the Module-0, was developed according to the same front-end design described in Section 5.
In Figure 23, the rendering of the two-channel front-end board prototype with 8 SiPMs and 2 crystals is shown.

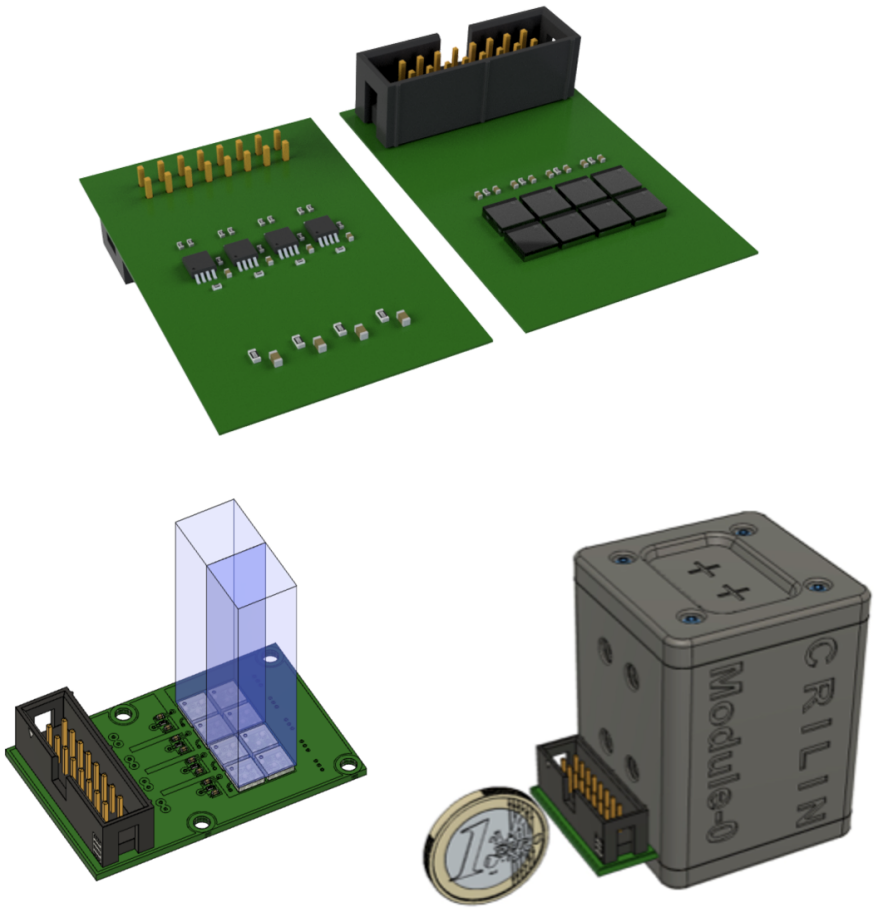

Figure 23: Rendering of the two-channel front end board prototype with 8 SiPMs and 2 crystals; PCB bottom (top left) and top view (top right), crystals installed (bottom left), Module-0 prototype.

The Module-0 was produced so as to characterise in detail the response of crystals and photosensors, with a focus on the time resolution evaluation with MIPs. Indeed, by relying on the first crystal as a trigger for cosmic rays, the charge and time resolution of the second can be evaluated using MIPs. A detailed study will be carried out to evaluate the timing resolution either using a single SiPM series, or with both of them. In the latter case, the timing resolution can be evaluated as the standard deviation of the distribution obtained by plotting the ratios of signal times, relative to the two SiPM series reading out the same crystal, and thus independently of any external timing reference.
Additionally, the performance of the system with respect to other design elements will be evaluated and validated, such as the optical coupling between SiPMs and crystals. For the latter, coupling with optical grease or silicone resin will be evaluated against the pre-

ferred option of direct coupling via an air gap and without the use of any optical coupling medium. Also, the optical cross talk between the two crystals will be evaluated, by relying again on cosmic rays measurements.
At the moment of editing, the Module-0 production is ongoing. Three electronics boards will be ready at the end of May 2021. Alignment and parallelism of the SiPMs assembly will be verified via Coordinate Measuring Machine (CMM) at Laboratori Nazionali di Frascati (LNF) of INFN. The requirements are very stringent, as the overall misalignment due to SiPM placement and reflow procedures should be inferior to 100 μm. The Artel company has been selected as the manufacturer and assembler of the boards. Test beams with electrons on this prototype are due in July 2021 at the new Beam Test Facility (BTF [16]) of LNF, along with studies using Cosmic Rays. The thus obtained results will drive the choice for the production of the final configuration and will be used to validate our electronics design.

7 Conclusion

The Crilin design wants to overcome the classic rigid distinction between homogeneous and sampling calorimeters, trying to establish a good compromise between the two in order to optimize the requirements in view of a future Muon Collider. Before the construction of the final prototype the single components were evaluated:

- Irradiation studies of Crystals and SiPMs are over and a dedicated paper will be submitted before the end of June 2021;
- Module-0 will be ready before the end of May 2021 and a dedicated Test Beam is scheduled at BTF with 500 MeV electrons in June/July 2021.

A Crilin prototype, composed of 2 layers of 9 crystals each and operating at 0 °C , will be built before the end of the year (December 2021). Our goal is to test its performance with 500 MeV electrons at BTF and with a high energy beam ($>$ 20 GeV) at CERN in 2022.

8 Acknowledgements

This work was born as an RD of detectors roadmap for a future muon collider and it is mainly supported by the RD_MUCOL collaboration of INFN Gruppo1. The authors wish to thank the LNF Division Research and SPCM departments for their technical and logistic support and are grateful to the people in Enea Casaccia and Enea FNG facilities for their extensive collaboration during the irradiation campaign of crystals and photosensors.

References

[1] Siccas website, `http://www.siccas.com/`

[2] Hamamatsu website,
https://www.hamamatsu.com/resources/pdf/ssd/s14160_s14161_series_kapd1064e.pdf

[3]] N. Bartosik et al., Detector and Physics Performance at a Muon Collider, JINST 15 P05001 (2020),doi: https://doi.org/10.1088/1748-0221/15/05/P05001.

[4] F. Abusalma et al., Expression of Interest for Evolution of the Mu2e Experiment,FERMILAB-FN-1052 FERMILAB-EOI-2018-01 (2018).

[5] P. Kozma et al., Radiation resistivity of PbF2 crystals, Nucl.Instrum.Meth.A 484 (2002) 149-152, doi:https://doi.org/10.1016/S0168-9002(01)02011-3

[6] A. Frankenthal et al., Characterization and performance of PADME's Cherenkov-based small-angle calorimeter, Nucl.Instrum.Meth.A 919 (2019) 89-97, doi: https://doi.org/10.1016/j.nima.2018.12.035.

[7] Ren Guo-Hao et a, Chinese Phys. Lett. 31 086102 (2014).

[8]] R.Y. Zhu, Radiation damage in scintillating crystals, NIM A Vol. 413 (1998) Issues 2-3, doi: 10.1016/S0168-9002(98)00498-7.

[9]] M. Cordelli et al.,Neutron irradiation test of Hamamatsu, SensL and AdvanSiD UV-extended SiPMs, Jinst 13 T03005 (2018), doi: https://doi.org/10.1088/1748-0221/13/03/T03005.

[10] Brochure Calliope,
https://www.enea.it/it/seguici/pubblicazioni/pdf-opuscoli/calliope.pdf

[11] FNG website,
http://www.fusione.enea.it/LABORATORIES/Tec/FNG.html.it

[12] PerkinElmer website,
https://www.perkinelmer.com/CMSResources/Images/44-74450BRO_LAMBDA8509501050.pdf

[13] P. Achenbach et al, Radiation resistance and optical properties of lead fluoride Cherenkov crystals, Nucl.Instrum.Meth.A 416 (1998) 357–363. doi: https://doi.org/10.1016/S0168-9002(98)00748-7

[14] Maxim website,
https://datasheets.maximintegrated.com/en/ds/MAX6335-MAX6337.pdf

[15] https://www.avx.com/products/passive-micro-components-pmc/q-bridge-thermal-conductor/

[16] B. Buonomo et al., The Frascati LINAC Beam-Test Facility (BTF) Performance and Upgrades, IBIC2016 (2017) 395-398, doi: 10.18429/JACoW-IBIC2016-TUPG29.

[17] http://www.mcstas.org/.